JOURNAL OF SOLID STATE CHEMISTRY 50, 335–361 (1983)

Electron Microscopic Studies of Modulated Structures in (Au, Ag) Te_2: Part II. Sylvanite $AgAuTe_4$

G. VAN TENDELOO, P. GREGORIADES,* AND S. AMELINCKX†

Rijksuniversitair Centrum Antwerpen, Groenenborgerlaan 171, B-2020 Antwerp, Belgium

Received June 6, 1983

Sylvanite ($AuAgTe_4$) occurs under two forms at room temperature. Ideal sylvanite has a commensurate modulated superstructure of calaverite. The second form is an incommensurate modulated structure. The modulation is due to periodic displacements from the ideal atom positions, occupied in the commensurate form, and to the presence of periodic antiphase boundaries. The two structural modulations are closely coupled however and occur along almost parallel sets of planes. It is believed that the incommensurability is related to deviations from the ideal gold–silver ratio. The antiphase boundaries provide a means to incorporate deviations from the ideal Au–Ag ratio without changing the deformation modulation period. These conclusions were reached on the basis of the combined use of electron diffraction, electron microscopy, and computer simulation of the high resolution images.

1. Introduction

In Part I of this work (*1*) we discussed the structural features of calaverite and we demonstrated that in a wide temperature range calaverite has an incommensurate modulated structure. In the present paper we report on a similar study in sylvanite, which has the ideal composition (Ag Au)Te_4. Use is made of electron diffraction, electron microscopy, and image simulation. We shall see that this material exhibits a remarkable coupling between deformation modulation and modulation by periodic antiphase boundaries, not previously found in any material.

2. Preparation of Material and Specimens

The material was prepared by melting together the constituent elements, in the required proportions like in the case of calaverite. Also the specimen preparation was the same, i.e., small fragments were obtained by crushing. The material cleaves easily along the (010) plane and most specimens are therefore oriented with this plane parallel to the supporting film. Since the cleavage plane is not as pronounced as in other layer structures of the CdI_2 type different orientations occur frequently and allow to image different sections at high resolution.

3. The Crystal Structure

Sylvanite is to a first approximation a superstructure of calaverite resulting from the ordering of gold and silver (*2*). Along the *a* axis of calaverite, which is parallel to the *c* axis of sylvanite, gold and silver atoms alternate in projection (Fig. 1). This means

* On leave from University of Thessaloniki, Greece.
† Also at SCK-CEN, Boeretang, B-2400 Mol, Belgium.

0022-4596/83 $3.00

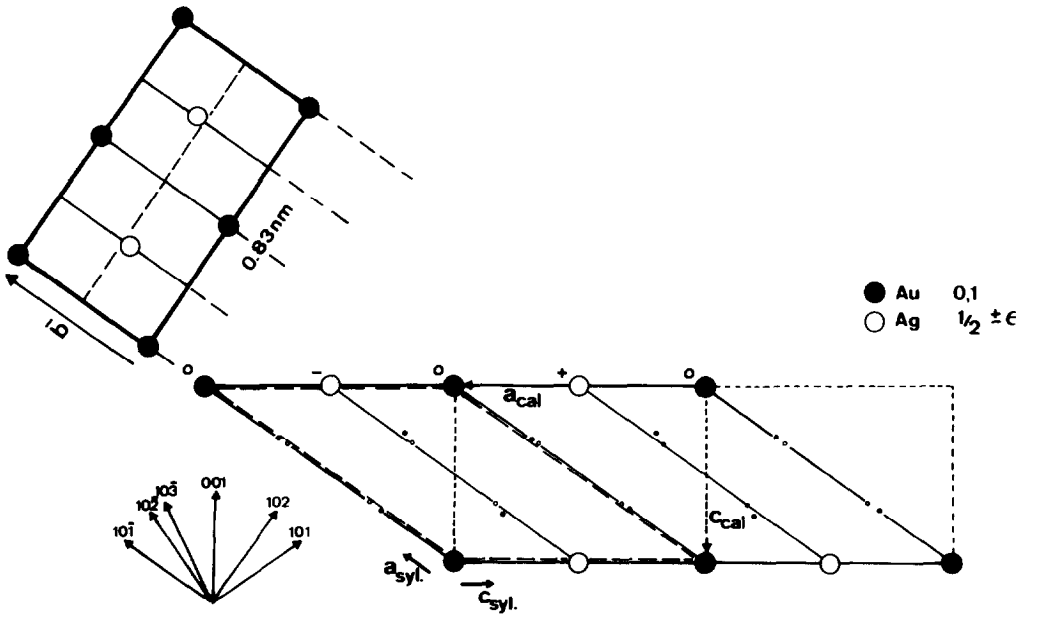

FIG. 1. (a) Crystal structure of sylvanite projected on the (010) plane (after Tunell and Pauling (*1*)). The conventional unit cell is shown in full line. The dotted line shows an alternative unit cell which consists of two juxtaposed calaverite unit cells. The small full dots represent the actuel Te position, as compared to the ideal ones, shown as open dots. The silver atoms along lines marked + are displaced upwards and those along lines marked − are displaced downwards. (b) Side view of the sylvanite structure along the $\bar{a}_{sylv}$ direction, which is also the $[10\bar{1})_{cal}$ direction. The displacements of the silver atoms are exaggerated.

also that along the *b* direction gold and silver containing layers alternate; this is represented in the side view of Fig. 1. The unit cell can be chosen, either as represented by the full line in Fig. 1 (and also in Table I of Part I), or as shown by the dotted line. From the latter choice it becomes evident that the sylvanite unit cell approximately consists in projection of two juxtaposed unit cells of calaverite. The base vectors of the unit cell shown in full lines are related to those of calaverite by the relation

$$\begin{bmatrix} \bar{a} \\ \bar{b} \\ \bar{c} \end{bmatrix}_{\text{sylvanite}} = \begin{bmatrix} +1 & 0 & -1 \\ 0 & 1 & 0 \\ -2 & 0 & 0 \end{bmatrix} \begin{bmatrix} \bar{a} \\ \bar{b} \\ \bar{c} \end{bmatrix}_{\text{calaverite}}$$

The structure of sylvanite is in a sense a commensurate modulated structure since the levels of the silver atoms are not exactly 0.5 *b*, but alternatively 0.433 *b* and 0.567 *b* along a row parallel with the c_{sylv} direction. The silver atoms are thus arranged according to a wave pattern with polarization vector along the *b* direction and wavevector perpendicular to the $(101)_{cal}$ planes. In a given $(101)_{cal}$ plane all silver atoms are at the same level. Also the tellurium atoms occupy positions which deviate somewhat from the ideal ones. The unit mesh in the b projection of the pattern of displacements of the silver atoms determines the unit cell. The unit mesh of the tellurium arrangement, shown in double lines, on the other hand, is only half of the size of the sylvanite unit cell. In Fig. 1 the small open circles represent the ideal tellurium positions and the small full circles the actual ones. Both

modulation patterns are coupled, of course. The tellurium atoms tend to have a coordination around a silver atom which is somewhat different from that around a gold atom (*2*). The planes of "equal phase" are the $(101)_{cal}$ planes, which are approximately also the planes of equal phase in the modulated calaverite structure. As we shall see below closely related incommensurate diffraction patterns occur in nonstoichiometric sylvanite and in calaverite; this strongly suggests a relation between these two modulated structures.

4. Reciprocal Lattice and Diffraction Pattern

4.1. Ideal Structure[1]

Four sections of reciprocal space are shown in Fig. 2. In Fig. 2a the $[010]_{sylv}$ zone corresponding with a [110] direction of the primitive quasi-cubic lattice is shown; the mesh shape is very nearly rectangular but with only half the size of the rectangles in the corresponding pattern for calaverite (Part I). As compared to the latter pattern weak spots now appear in the centers of the longest edges of the rectangles of Fig. 2a: these are due to the ordering of gold and silver which leads in this projection to doubling of one of the edges of the projected unit cell, as discussed in Section 3.

The [100] zone parallel with the pseudocube direction (Fig. 2c) has the same pseudo-square aspect as in calaverite except for a row of three spots dividing the diagonal of the square in four parts leading to the c_{sylv} axis represented in Fig. 1. Whereas the 001 and 003 spots are absent in the [010] zone they are present here as a result of double diffraction. The fourfold periodicity is a consequence of the fact that the silver atoms have suffered displacements from the ideal positions along the [010] direction, doubling the period in the [001] direction, whereas the unit cell of the tellurium lattice has only half the size of that of the silver lattice. This is, of course, reflected in the systematic extinctions of the space group in the [010] zone; only reflections $h0l$ with l = even are present.

Figure 2b represents the $[131]_{sylv}$ zone perpendicular to the pseudo-close packed planes. Again as in calaverite the pattern of basic spots deviates only slightly from a perfectly hexagonal one. The commensurate fourfold superperiod is quite apparent now.

Finally Fig. 2d shows the $[2\bar{2}1]_{sylv}$ zone; along the densest rows of spots again weak and intense spots alternate. In adjacent rows the alternations of weak and intense spots are in antiphase. The weaker spots are again due to ordering of silver and gold. We studied several other sections of reciprocal space and found no disagreement with the results of Tunell and Pauling (*1*). There is therefore no reason to question the structure of ideal sylvanite $AuAgTe_4$ as proposed by these authors.

4.2. Reciprocal Lattice of Deformation Modulated Structures

In Ref. (*3*) it was shown that in deformation modulated structures the intensity of satellite spots is proportional to the intensity of the basic spots, with diffraction vector $\bar{H}$, from which they are derived, and furthermore proportional to $[(\bar{H} + \bar{q}) \cdot \bar{R}]^2$ where $\bar{R}$ is the polarization vector of the deformation wave and $\bar{q}$ the wavevector of the considered harmonic. This means that satellite spots derived from high order basic spots, i.e., with a large $\bar{H}$ vector, will have intensities which, relative to those of the basic spots, are much larger. This trend is clearly visible in all the diffraction patterns which will be discussed below; proving that the satellites have to be attributed primarily to a deformation modulated structure.

[1] In this paragraph sylvanite indices are used.

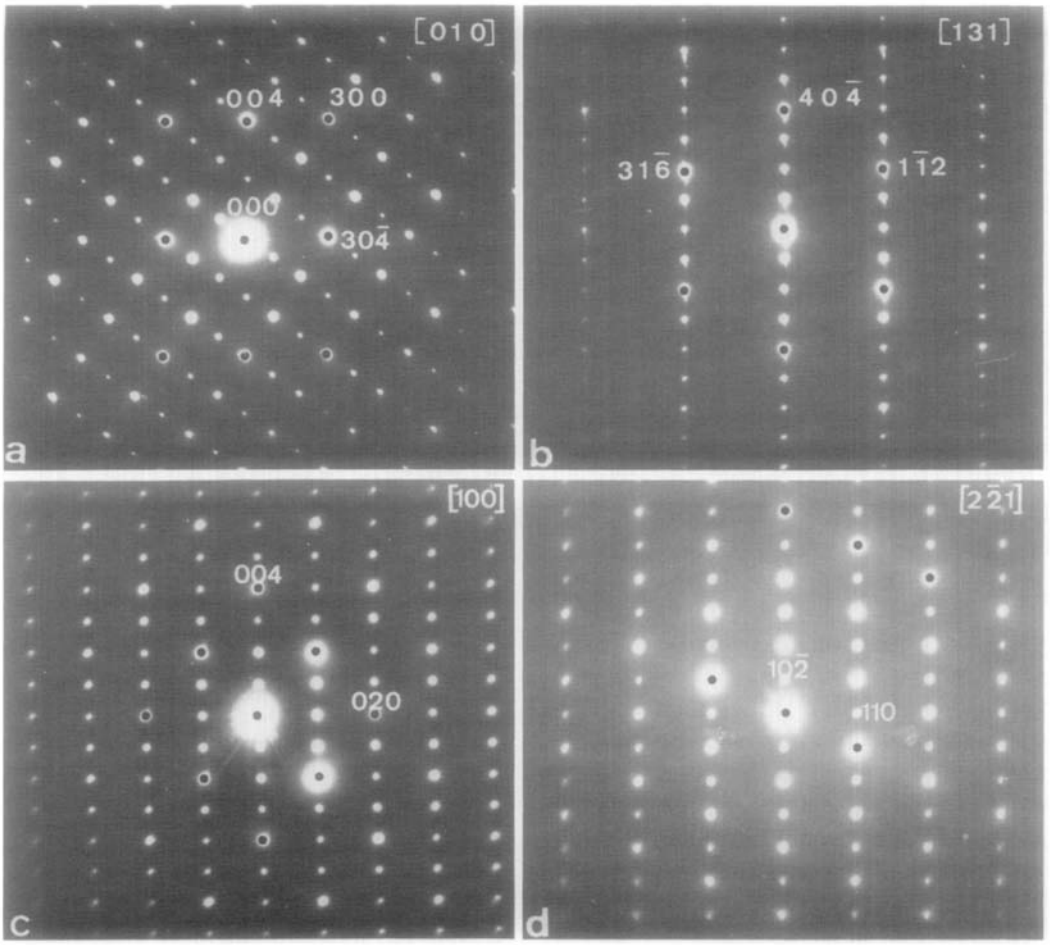

FIG. 2. Four sections of reciprocal space of commensurate sylvanite indexed with respect to the sylvanite lattice. (a) [010] zone pattern: note the alternation of weak and strong spots along the [10$\bar{1}$] direction; the weak spots are due to ordering. Note also the absence of 001 and 003 which is related to the Ag displacements parallel with [010]. (b) [131] zone pattern; pseudo-hexagonal section of the quasi-cubic lattice. Note the fourfold periodicity. (c) [100] zone. Note the presence of 001 and 003 in this zone due to double diffraction. (d) [2$\bar{2}$1] zone. Note the alternation of weak and strong reflections in the diffraction [10$\bar{2}$] direction.

Since several satellites are present the deformation wave contains several harmonics.

Satellites of a given order, i.e., a given q vector, will be absent in a given zone if the polarization vector of the corresponding harmonic is perpendicular to all diffraction vectors in that zone, i.e., if the polarization vector is parallel with the zone axis. This follows directly from the fact that the intensity is porportional to $|(\bar{H} + q) \cdot \bar{R}|^2$, i.e., to the square of the projection of $\bar{R}$ on $\bar{H} + \bar{q}$.

4.3. Deviations from the Simple Pattern

In this paragraph we refer to material with an average composition $AuAgTe_4$; it is probable that locally the composition is somewhat different. To facilitate compari-

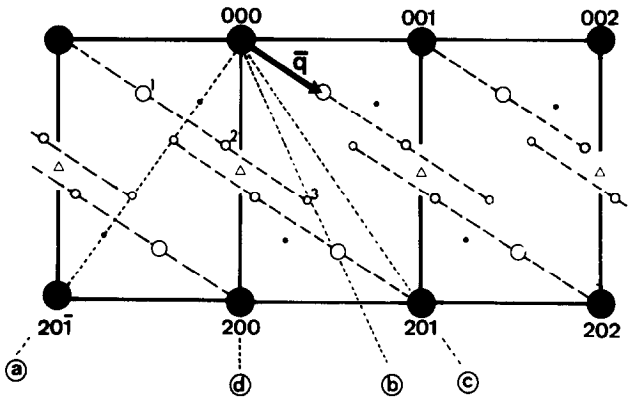

FIG. 3. Schematic representation of the [010] section of the reciprocal lattice of the incommensurate sylvanite structure. Large full circles represent "basic" reflections due to the primitive pseudo-cubic lattice. Small triangles refer to the commensurate sylvanite reflections, which are replaced by the pairs of medium size circles. Open circles of decreasing size represent first and third order satellites absent in this section. The indices refer to the calaverite lattice. The small full dots may be produced by double diffraction in certain sections. The order of the satellites is indicated 1, 2, 3, and 4; the spots may also be produced by double diffraction. Four different sections normal to the plane shown are indicated as a, b, and c; they correspond to Fig. 7, and to Figs. 4f, e, and c, respectively.

son with the calaverite structure, we refer the indices to the calaverite unit cell unless otherwise stated.

In most sylvanite crystals similar satellite sequences occur as in calaverite. Along the $[010]_{cal}$ zone the spots $h0l$ with h = odd, and which are associated with the ordering of gold and silver are in many crystals replaced by the satellite pairs already described for calaverite. The basic spots also exhibit satellites; these may either be due to double diffraction or to the fourth order satellites (Fig. 3). The measurements do not allow to distinguish between these two possibilities. The second order satellites are represented by medium size open circles in Fig. 3. In sylvanite these spots have a intensity larger than the corresponding spots in calaverite, as compared to the intensity of the basic spots. When tilting away from the [010] zone other satellite sequences make their appearance.

Figure 4 reproduces six sections of reciprocal space. In all of them satellite spots can be recognized next to the basic spots, due to the pseudo-cubic basic lattice. The detailed interpretation of such patterns is not trivial. The most relevant section is the one shown in Fig. 4d, i.e., the $[10\bar{1}]_{cal}$ section. The distance from the origin to the $(202)_{cal}$ spot is divided in about 4.5 to 4.6 equal parts; there is a small orientation but a large spacing anomaly suggesting a noncommensurate structure. This section is the incommensurate version of the $[100]_{sylv}$ section of Fig. 2c where the distance between the $[004]_{sylv}$ spot and the origin is divided in exactly four equal parts.

The [202] satellite sequences are particularly well observable in the $\bar{1}11$ section shown in Fig. 5. Up to eight satellite spots occur in one linear sequence. The relations with their basic spots are indicated explicitely in the inset of Fig. 5.

Returning to the 010 section (Fig. 4a) one notes that the 202 spot belongs to this section; so why are the 202 sequences of satellites not visible? The same reason as in the case of calaverite has to be invoked. The structure of commensurate sylvanite con-

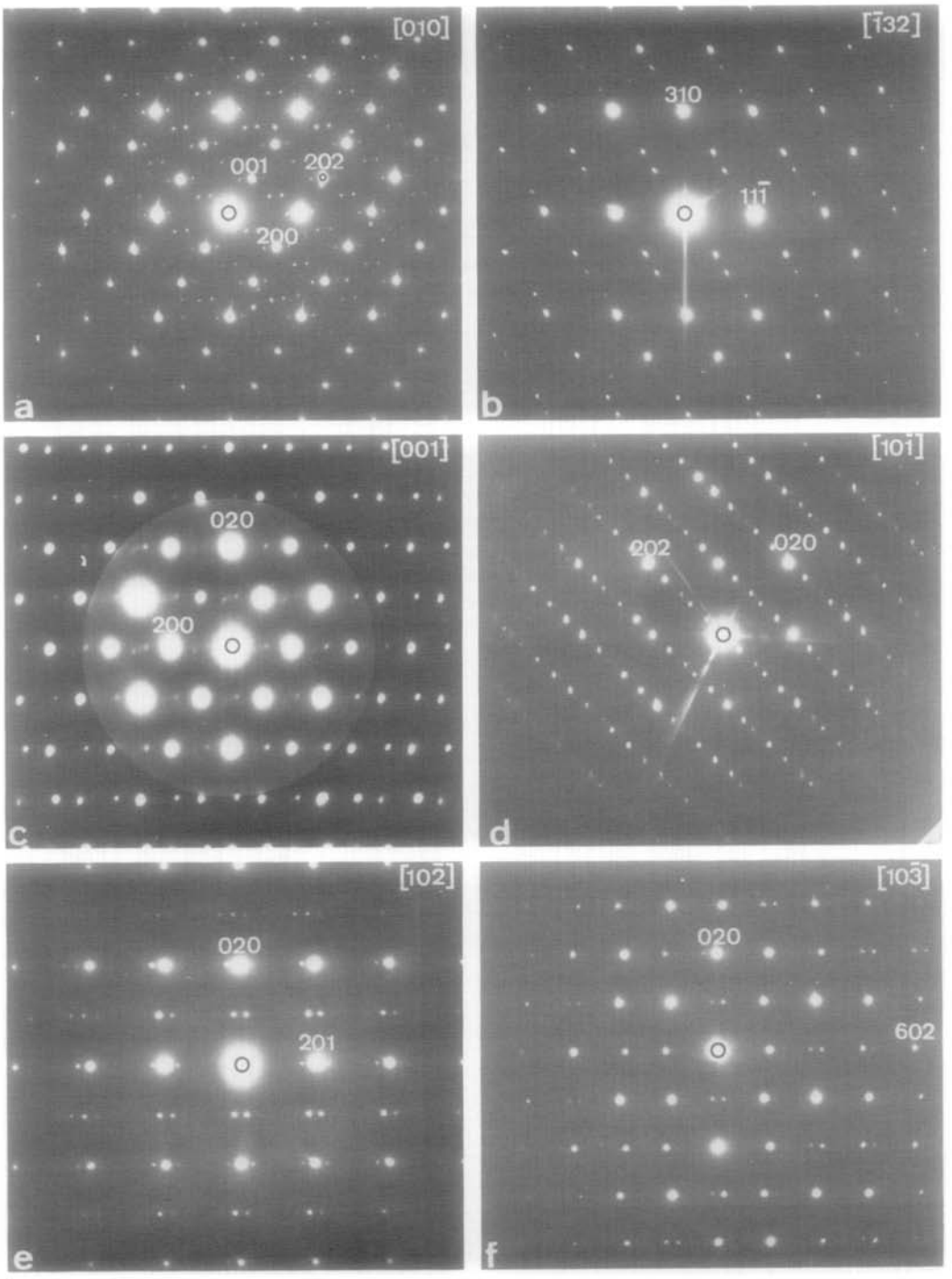

FIG. 4. Six sections of the reciprocal lattice of the incommensurate sylvanite structure (calaverite indices). (a) [010] zone pattern. The pairs of weak spots are second order satellites. (see Fig. 3). (b) [$\bar{1}$32] zone pattern. (c) [001] zone pattern perpendicular to the close packed planes. Note that the satellites are relatively more intense at high order basic reflections. (d) [10$\bar{1}$] zone pattern. The basic spots form a pseudo square arrangement. One diagonal of the squares is divided into ~4.5 equal parts. The orientation anomaly is small in this section. (e) [10$\bar{2}$] zone pattern. Note the pairs of spots in the [201] direction: see line c in Fig. 3. (f) [10$\bar{3}$] zone pattern. An analysis of the row of spots between the origin and the 002 spot is illustrated schematically in Fig. 6. The spot pairs are produced by basic spots and by satellites of different order originating from different basic reflections. See also line b in Fig. 3.

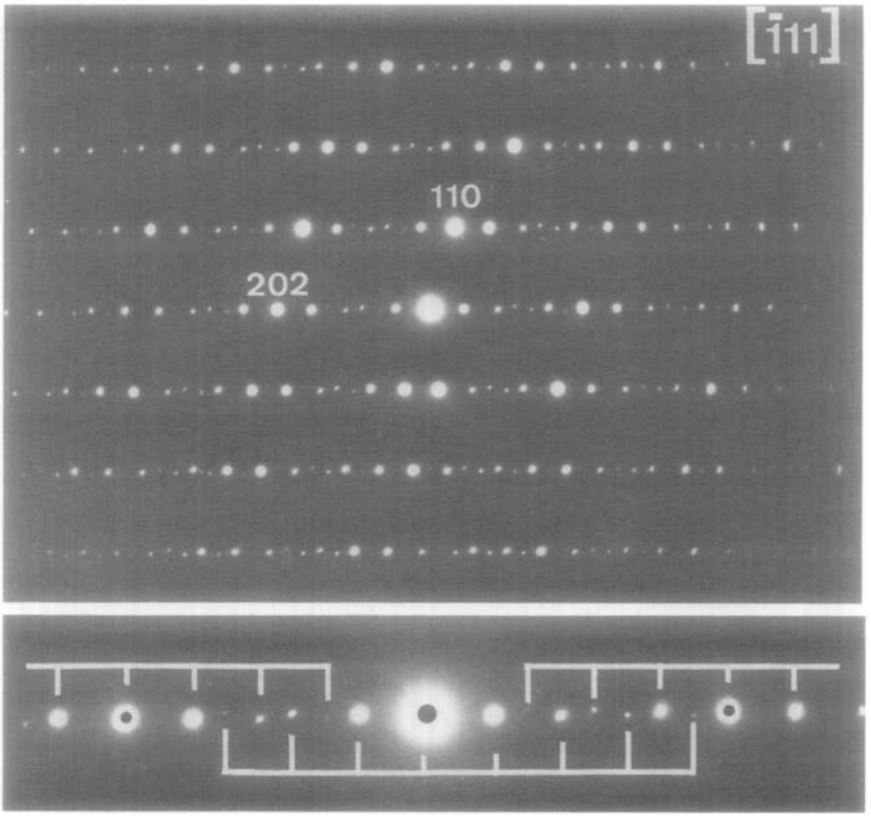

FIG. 5. Particularly well-developed satellite sequences in the [$\bar{1}$11] zone. Up to eight satellites belonging to the same linear sequence are visible.

firms in a sense the suggestion made in Part I, i.e., that the presence of the even order satellites is due to the particular displacement pattern. The satellites due to the modulation of the heavy metal positions should *all* be absent in the [010] zone if, as in commensurate sylvanite, all displacements are parallel with the [010] direction. On the other hand, the displacements of the Te atoms from their ideal lattice positions have a component parallel with the (010) plane and have only half the period of the heavy metal displacements. As a result only the even order satellites appear in the [010] section; in all other sections the different orders appear. The [010] section is represented schematically in Fig. 3, only the even order satellites are actually present in this section; the different open circles of decreasing size represent satellites of increasing order of which the odd orders are absent in the [010] section but appear in other sections.

In the [001] zone the linear sequences of satellites intersect the reciprocal lattice plane; this is obvious from Fig. 4c leading to a single satellite spot, or to weak spot pairs. The doublet of satellites which is prominently visible in the [010] section is also weakly visible here around the origin, one satellite being in fact situated above and the other one below the excited reciprocal lattice plane line d in Fig. 3. Further away from the origin, because of the curvature of Ewald's sphere, only one of these

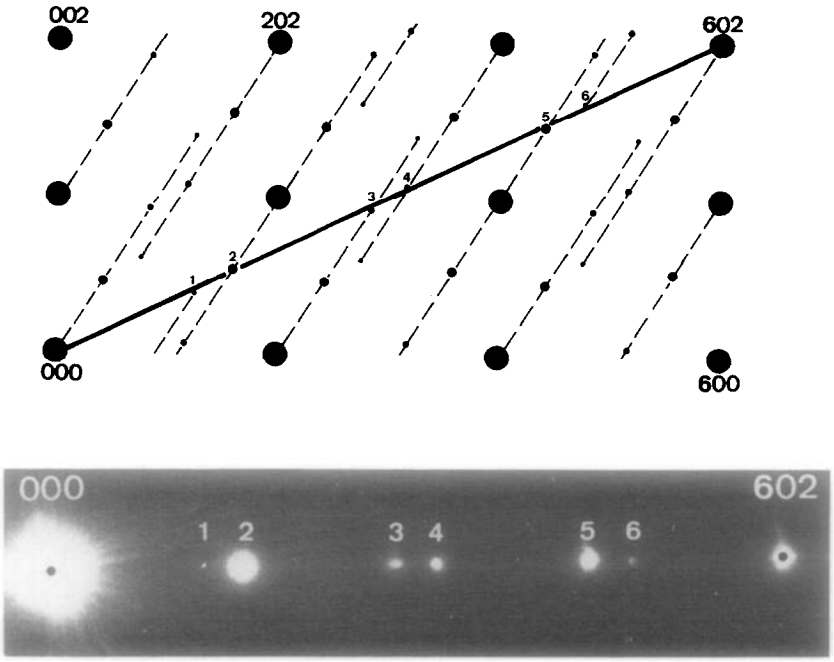

FIG. 6. Section through the reciprocal lattice of the incommensurate structure along a plane normal to the (010) plane and along the solid line produces the diffraction pattern of Fig. 4f. One line of spots is shown in the lower part of the drawing.

two satellites is strongly excited. This section reveals in a particularly striking manner the fact that the satellites associated with high order basic spots are relatively much more intense, which is a typical feature for deformation modulated structures. In this particular case it is also a consequence of the curvature of Ewald's sphere.

In the other sections, such as [10$\bar{2}$] (Fig. 4e) and [10$\bar{3}$] (Fig. 4f), only close pairs of satellite spots are visible. It is not obvious whether a spot is due to the basic structure or has to be considered as a satellite spot. The analysis of these patterns is far from trivial and cannot be done without performing tilting experiments over well-defined angles. One spot sequence in a section of the reciprocal lattice by a plane normal to the (010) plane and along line b in Fig. 3 or the heavy line indicated in Fig. 6, is reproduced at higher magnification in the lower part of Fig. 6. The sequence of spots as observed in Fig. 4f is clearly well reproduced. Also the relative intensities are well obeyed. It turns out that first, second, and third order satellites belonging to different sequences contribute to this pattern. The pattern of Fig. 4e results if the trace of Ewald's sphere coincides with line c (Fig. 3) and is perpendicular to the (010) plane.

The four diffraction patterns of Fig. 7 exhibit apparently a quite different sequence of satellites aligned along the [20$\bar{1}$] direction. On tilting it turns out that other sections of the same specimen exhibit the [202] rows of satellites also found in calaverite and in Fig. 4d. This means that these diffraction patterns are associated with the same modulated structure. With reference to line a in Fig. 3 it turns out that such spot

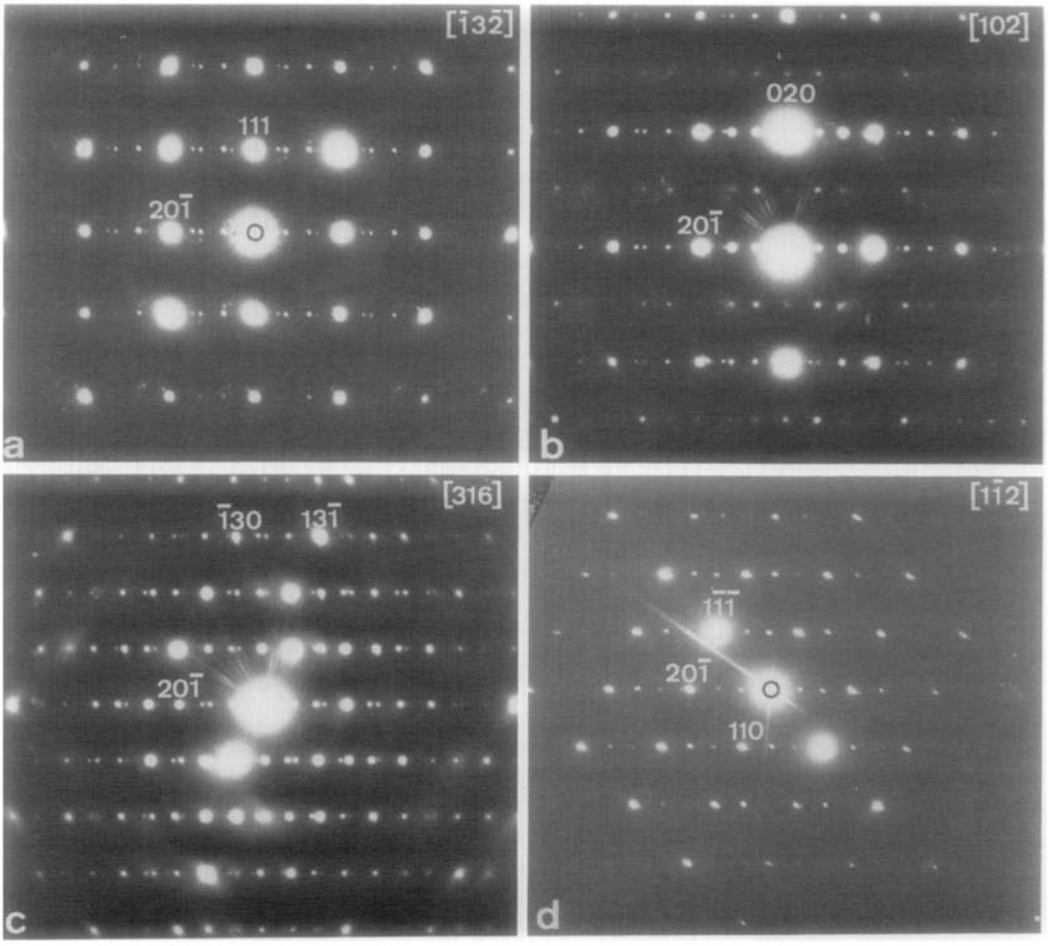

FIG. 7. Four different sections of reciprocal space containing the [20$\bar{1}$] sequence of satellites. For the origin of this sequence see line a in Fig. 3. (a) [1$\bar{3}\bar{2}$] zone pattern, (b) [102] zone pattern, (c) [316] zone pattern, (d) [11$\bar{2}$] zone pattern.

sequences can be interpreted in terms of satellites of different order, up to the third of the [202] sequences considered above.

5. High Resolution Images

5.1. Ideal Structure

Structure images along the [010] zone are shown in Fig. 8. They refer to regions of different thickness; the image is not essentially different from that of calaverite but the period in the *c* direction is twice that along the a direction in calaverite. The bright dots in Fig. 8b produce a pattern which has the right scale and configuration to represent all atom columns—gold and silver as well as tellurium atoms.

The image has the same period as the projected structure, although the difference between the dots representing gold and silver columns is very small; the true period is marked by a difference in spacing of the dots rather than by a difference in their intensity. In different parts of the specimen

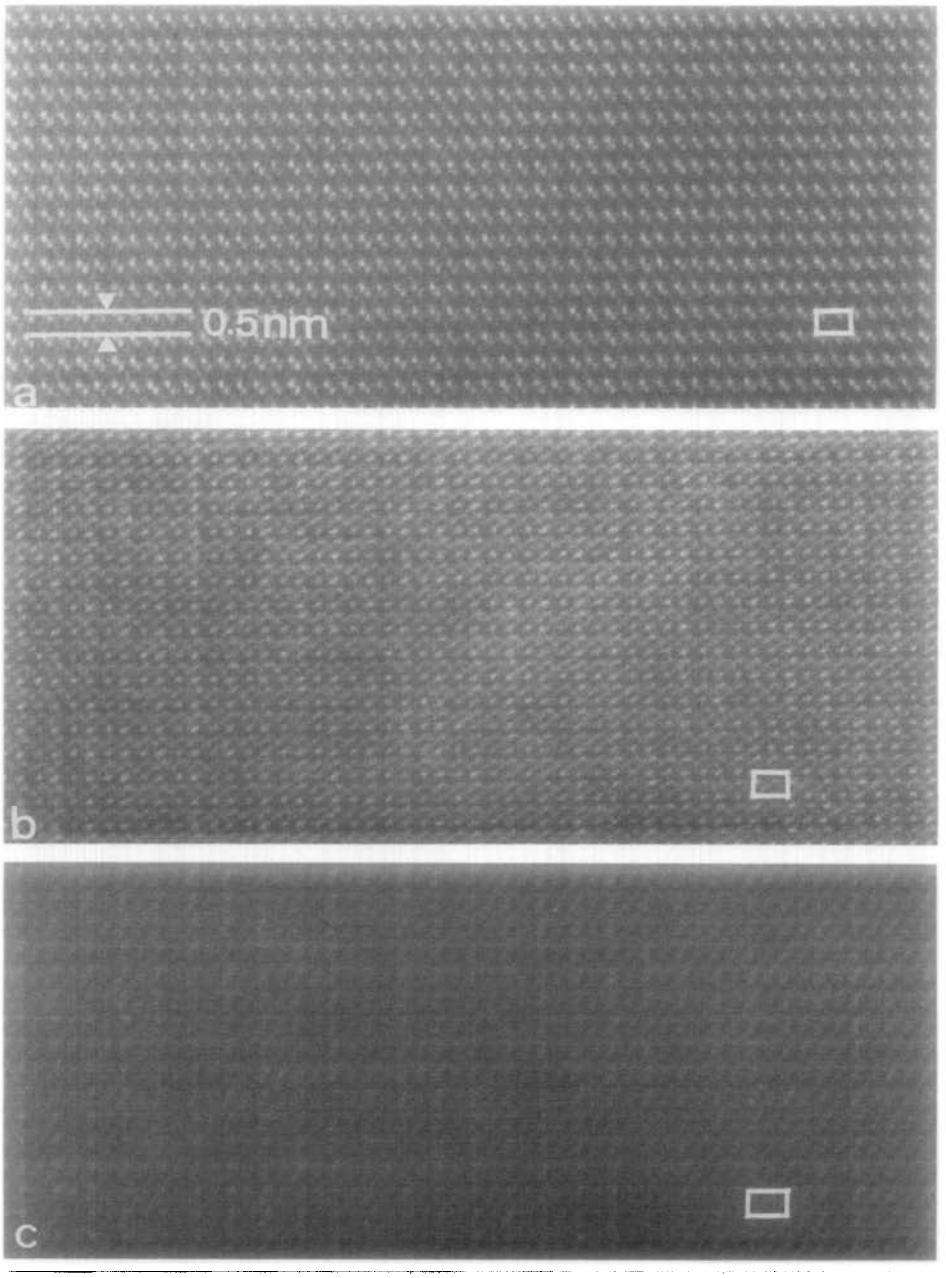

FIG. 8. High resolution images along the [010] zone of sylvanite. (a) Thick part: only the unit cell is outlined; gold and silver columns are visible. (b) Thin part: subunit cell detail. Tellurium columns are also visible. (c) Intermediate thickness. Compare with Fig. 20.

the image simplifies somewhat and the configuration of dots has now the configuration of the columns of gold and silver; the tellurium columns are practically invisible (Fig. 8d). The difference between gold and silver columns may become more pronounced

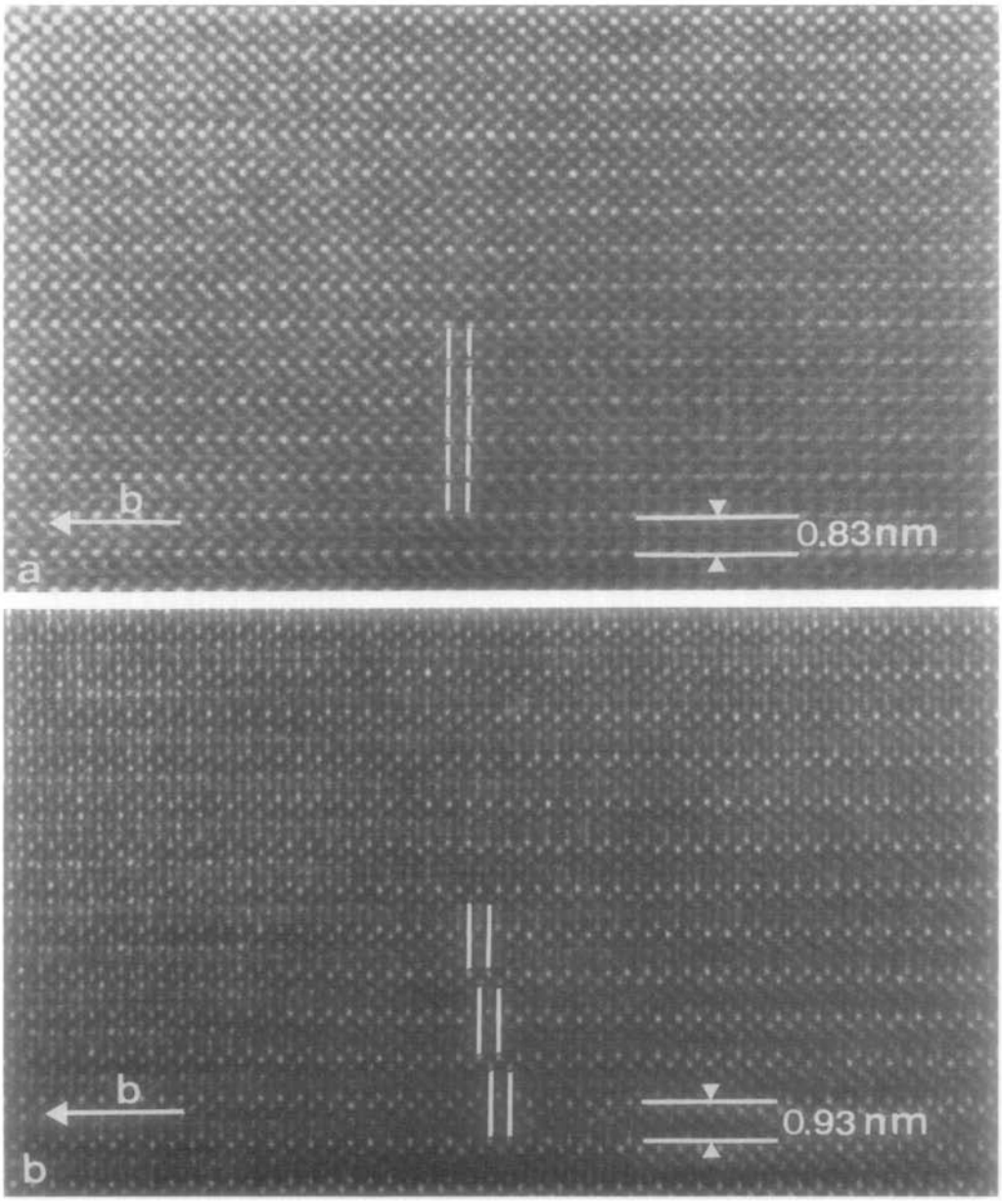

FIG. 9. View of the sylvanite structure along the $[10\bar{1}]_{cal}$ direction. (a) Commensurate structure (see diffraction pattern in Fig. 2c). The intensity modulation in the thick part reveals the true period. Separate $AuTe_2$ and $AgTe_2$ column can clearly be recognized following a pseudo-square pattern. A few unit cells are outlined. (b) Incommensurate phase (see diffraction pattern in Fig. 4d). The intensity modulation reveals again the true period, but also shows that antiphase boundaries occur. A few unit cells are outlined to illustrate the sideways shift. The orientation anomaly is also apparent when viewing the photograph along horizontal lines.

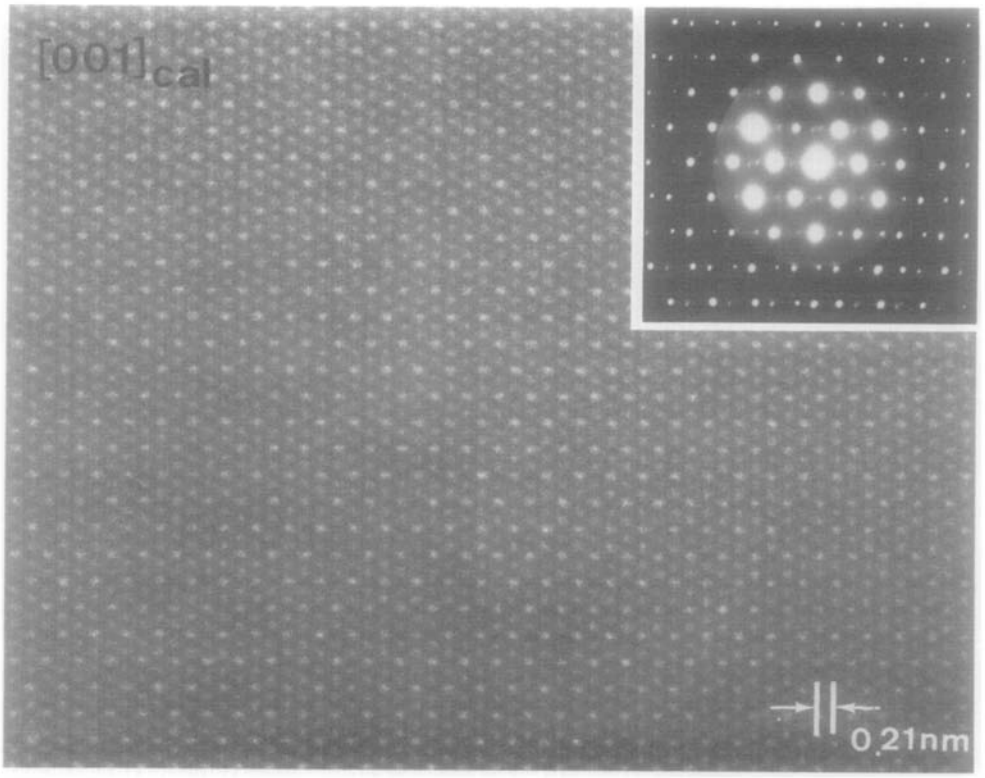

FIG. 10. Ideal sylvanite; view along the direction $[001]_{cal}$ perpendicular to the close packed planes (see diffraction pattern of Fig. 4c). The bright dots represent heavy metal columns and the weaker dots tellurium columns. Compare with Fig. 22.

and the doubling of the projected period can then be recognized more easily (Fig. 8c). The view along the $[100]_{sylv}$ direction (Fig. 9) is of particular interest. Along this direction the atoms occur in separate columns of $AuTe_2$ and $AgTe_2$ forming a centered pseudo-square arrangement, the corners of the squares formed for instance by gold–tellurium columns and the center by silver–tellurium columns (Fig. 9a). The image along this direction does in fact exhibit such a centered square pattern formed by dots of two different brightnesses. The true period in commensurate sylvanite, along the a^*_{sylv} direction, contains two such centered squares; in the thicker parts of the crystal this true period is revealed by dots of somewhat larger brightness. The projected unit cells are indicated in Fig. 9a.

Figure 10 exhibits the image observed along the pseudo-hexagonal $[001]^*_{cal}$ zone. The hexagonal arrangement contains dots of two different intensities. Along this zone the structure is a true column structure, i.e., all atoms along a column are of the same chemical nature. Each gold column is surrounded by six tellurium columns in the first shell, and three gold columns and three silver columns in the second shell of neighboring columns. There are thus two tellurium columns for one heavy atom column. It is therefore reasonable to associate the brightest dots with heavy atom columns and the weaker bright dots with tellurium

columns. This will be confirmed by the calculated images. As can be judged from the diffraction pattern in the inset of Fig. 10 this image was obtained from a modulated crystal; however, similar images are obtained from ideal sylvanite. This image does not exhibit any visible effect of the modulation. Also a difference between gold and silver containing columns is not apparent; this might be related to the fact that antiphase boundaries present along $(001)_{sylv}$ planes perturb the chemical composition of the columns; we shall see this further in detail.

Figure 11 represents a different pseudo-hexagonal projection, i.e., the $[131]^*_{sylv}$ zone. The configuration of bright dots is very nearly hexagonal. In the thin part of the specimen all dots have equal brightness; in the thicker part the spot brightness is modulated in accordance with the period deduced from the diffraction pattern of Fig. 2b. This image clearly suggests that commensurate sylvanite can also be considered as a modulated structure.

The diffraction pattern along the $[2\bar{2}1]_{cal}$ zone was reproduced in Fig. 2d. The corresponding image of Fig. 12 is of interest; it exhibits a centered elongated rectangular pattern of dots of two different intensities, which can be associated with the configuration of silver and gold containing columns. Tellurium atom columns are apparently not revealed as resolved dots under the conditions used in this image. The long period is 0.73 nm whereas the distance between spots along the dense rows is 0.3 nm. This image can be compared with the simulated structure images (inset, Fig. 12) at two dif-

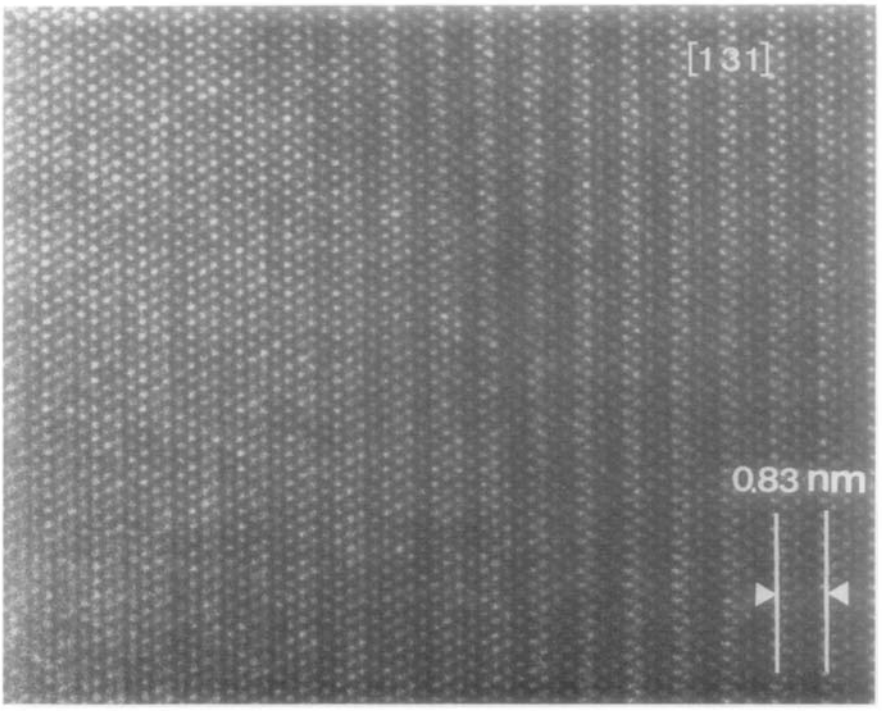

FIG. 11. Ideal sylvanite: view along the $[131]_{sylv}$ zone of the pseudo-close packed planes (see also diffraction pattern of Fig. 2b). Note the intensity modulation of the rows of bright dots; one period contains four rows of dots.

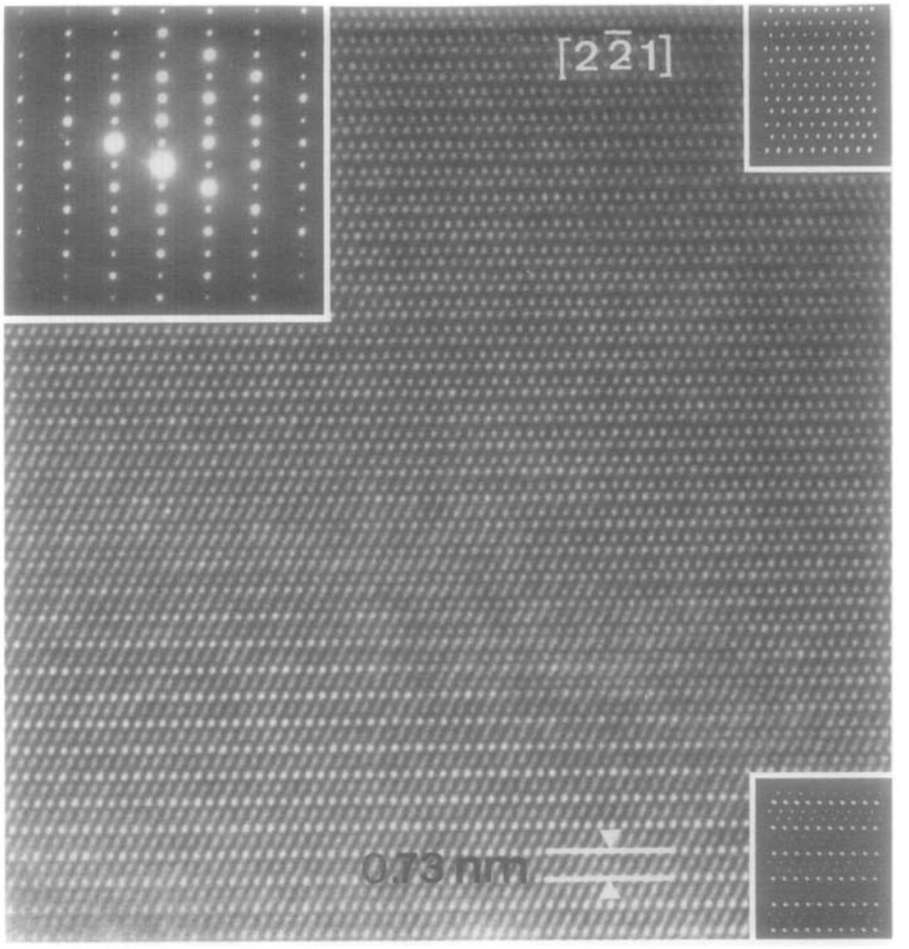

FIG. 12. View along the $[01\bar{1}]_{cal} \equiv [2\bar{2}1]_{sylv}$ zone. See also diffraction pattern of Fig. 2d and the diffraction pattern in the inset. The small insets are two simulated images along the same zone, at different thicknesses, at the same scale as the photograph.

ferent thicknesses. The diffraction patterns as well as the high resolution images are all consistent with the assumption that gold and silver order in the manner proposed by Tunell and Pauling (*1*). It is not clear whether or not this occurs in all specimens.

5.2. Incommensurate Structures

The image along the [010] zone is not essentially different from that of calaverite made along the same zone. The best visible modulation is again that due to the shortest q vector, connecting the two satellite spots. From the fact that only the weak second order satellites are present in this zone we expect that not much information on the nature of the modulated structure is to be obtained from images made along this zone.

Occasionally we found crystal fragments producing diffraction patterns in which the satellite pairs were exceptionally intense and where up to four equidistant satellites were present in the sequence, i.e., the small black dots of Fig. 3 were actually present. The images of such crystals exhibited rectangular arrangements of bright dots with

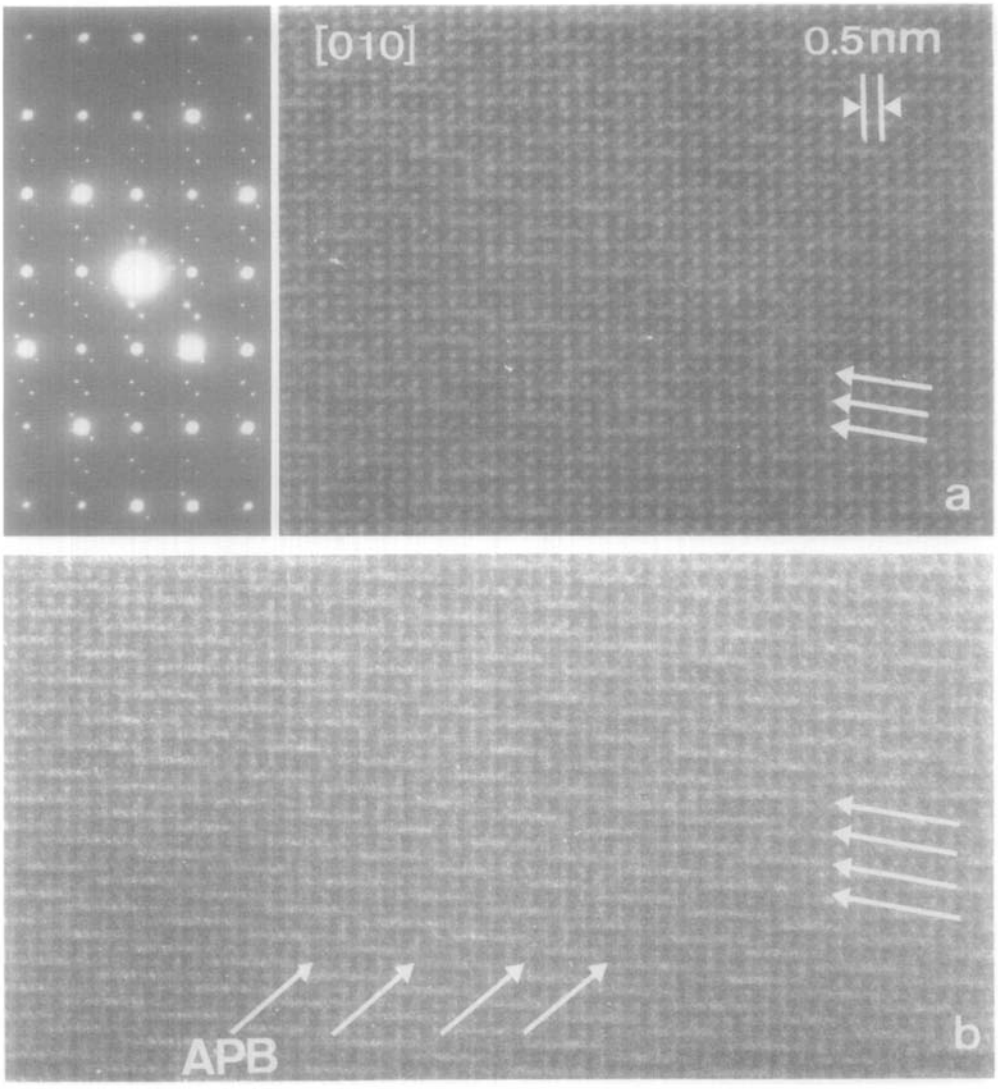

FIG. 13. High resolution image along the [010] zone of incommensurate sylvanite. The modulations are due to the presence of antiphase boundaries along $[101]_{cal}$ planes. Along such planes rows of silver columns interchange with gold columns (compare with Fig. 23).

the size and orientation of the heavy metal columns and which were rather strongly modulated in brightness (Fig. 13).

Along the [010] zone the crystal has a true column structure, i.e., gold and silver occur in separate columns. One therefore expects to see a difference between the two kinds of columns. This is actually the case; it is quite clearly visible that the intensity along the horizontal rows of dots varies periodically. The geometrical loci of the points of equal brightness are parallel equidistant straight lines which are roughly along the traces of $(202)_{cal}$ planes and which have a spacing of about 1.5 nm. Along these lines the brightness of the horizontal rows

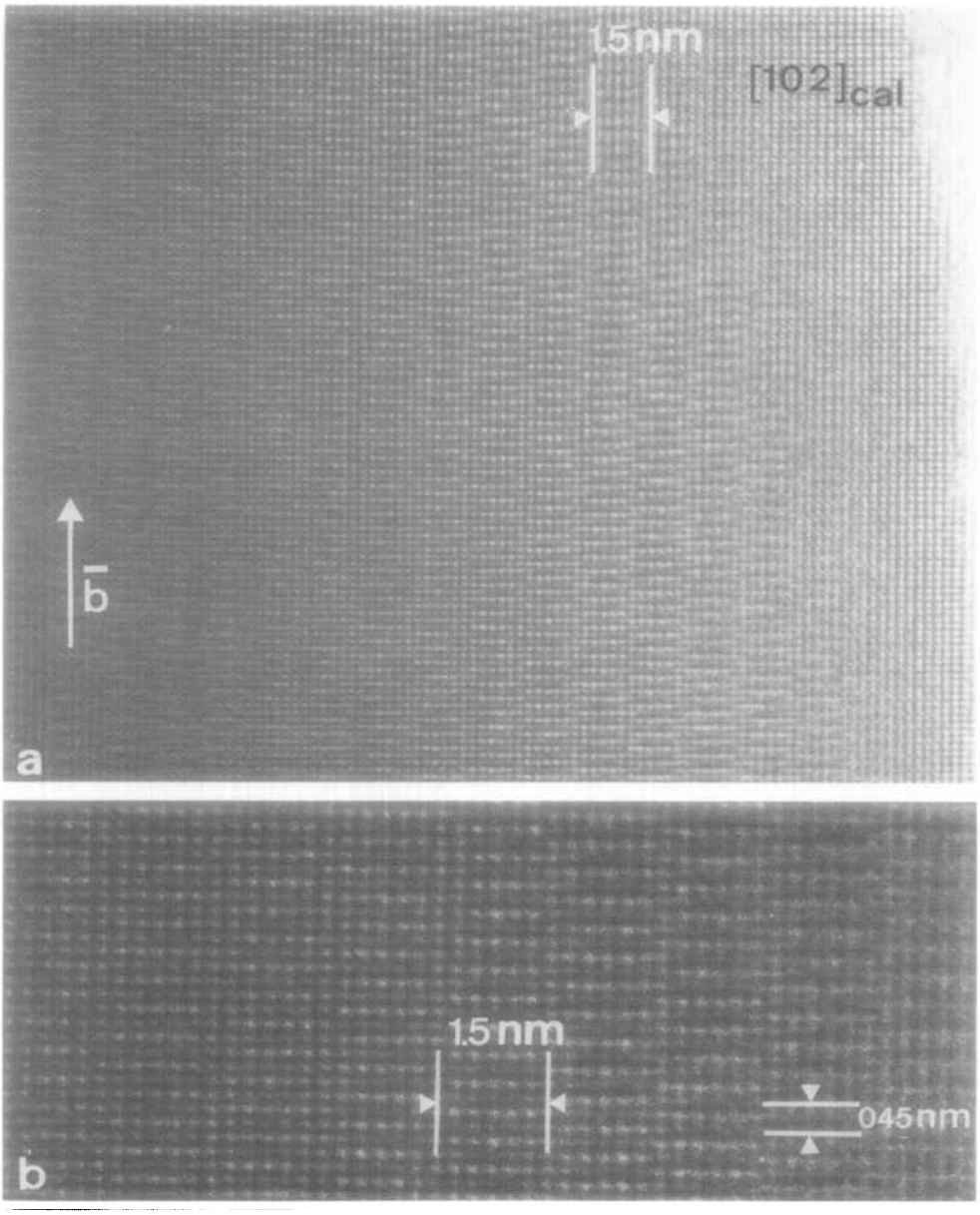

FIG. 14. View along the $[102]_{cal}$ zone. Note the presence of periodic antiphase boundaries roughly parallel with the *b* direction. The boundaries are not seen edge-on and have an apparent width.

of dots which are parallel with the [100] direction interchanges periodically. A segment of four or five bright dots becomes a segment of four or five less bright dots and vice versa. It is very suggestive to associate, e.g., the brightest dots with silver columns and the less bright dots with gold columns. The $(101)_{cal}$ traces would then be the traces of antiphase boundaries along which gold and silver columns are inter-

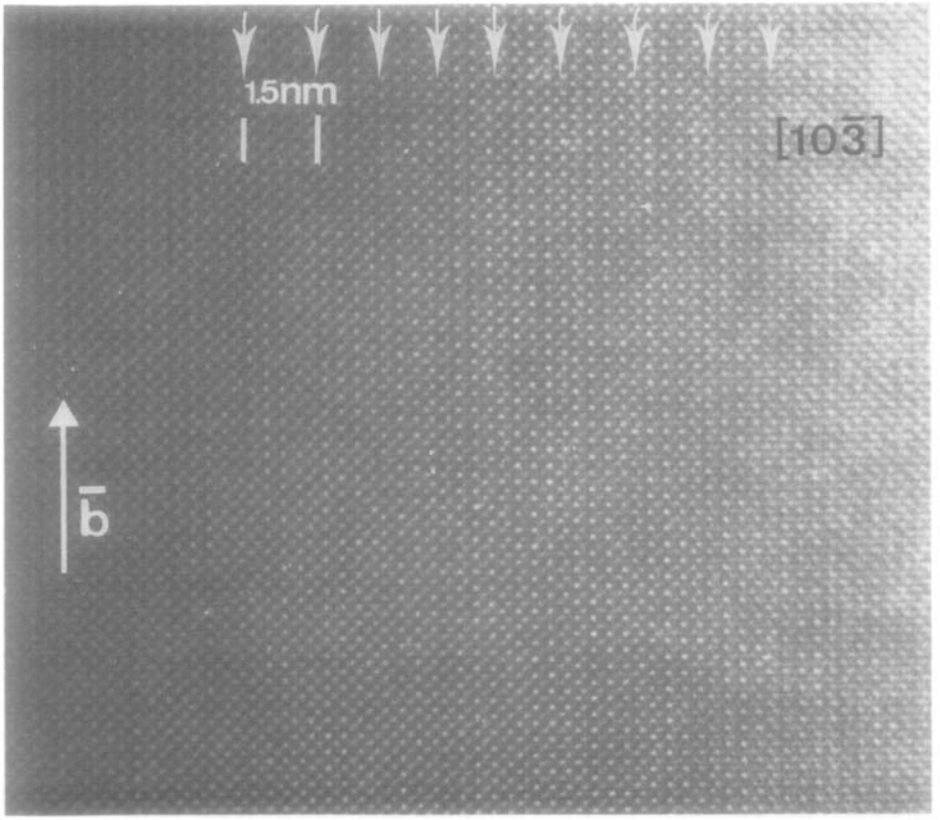

FIG. 15. View along the $[10\bar{3}]_{cal}$ zone. Note the presence of periodic antiphase boundaries roughly parallel with the *b* direction. The boundaries have a certain width either as a result of interleaving, or because they are not seen edge-on. The antiphase boundaries can best be observed by looking at the photograph under a glancing angle along horizontal lines.

changed. We shall see that also the other images confirm this interpretation.

High resolution images along the $[10\bar{2}]$ and $[10\bar{3}]$ zones reproduced in Figs. 14 and 15 also reveal an antiphase boundarylike structure. The images of Fig. 14 can be compared with the model of Fig. 16a. The brightest dots in Fig. 14 form a rectangular pattern. In the thinnest part the brightness of all dots is the same but in the thicker parts their intensity is modulated. Along horizontal lines, which are the traces of (010) planes, the brightness of the dots varies periodically. The changes in brightness occur along somewhat diffuse vertical lines, which are the traces of the antiphase boundaries. The spacing between the APB's as seen in this zone is of the order of 1.5 nm. The mesh size and shape of the pattern formed by the bright dots in the thin part is compatible with that of the pattern formed by the columns containing heavy metal atoms. It is therefore reasonable to consider the bright dots as representing gold and silver containing columns.

The image in the thicker parts then suggests that silver and gold containing layers alternate along the [010] direction and that a gold containing layer changes into a silver containing layer along the interfaces. This

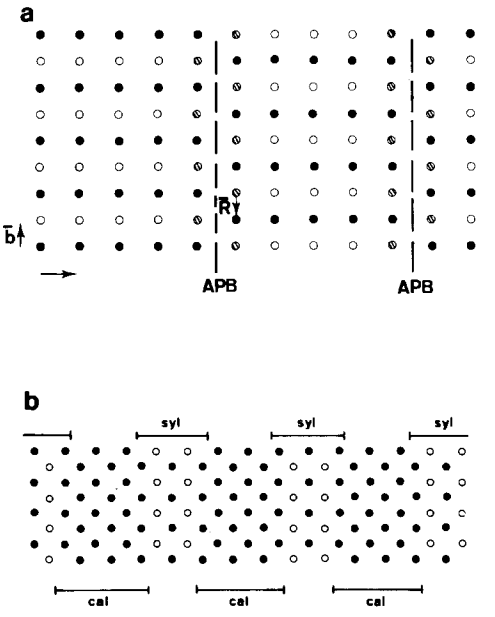

FIG. 16. (a) Model for the periodic antiphase boundary structure revealed in Fig. 13 as viewed along the $[10\bar{2}]_{cal}$ zone. The cross hatched columns may contain either silver or gold. (b) View along the $[10\bar{1}]_{cal}$ zone. Along the antiphase boundaries "interleaving" may occur in order to incorporate an excess of gold without changing the period.

is represented schematically in Fig. 16. Such interfaces have the character of antiphase boundaries. The period is consistent with that deduced from the diffraction pattern of Fig. 14. The antiphase boundaries are apparently not seen edge-on in this image; presumably they are inclined and therefore acquire a certain width in projection. It is also possible that some "interleaving" occurs, i.e., that along the interfaces the changeover from gold to silver does not occur strictly in a plane but more likely as represented in Fig. 16b. In this way appreciable deviations from the ideal gold–silver ratio can be incorporated in the crystal without changing the modulation period. An excess of gold could for instance give rise to a thin layer of calaverite along the interface (Fig. 16b).

The image along the $[10\bar{3}]$ (Fig. 15) zone reveals a somewhat similar aspect; the pattern now consists of bright dots forming centered squares with their edges parallel with the edges of the photograph. Along a horizontal row of dots, parallel with the *b* (010) planes, the brightness again varies periodically, the changes taking place along vertical lines indicated by arrows in Fig. 15. The same phenomenon of interleaving takes place. Both these images are consistent with the model for the antiphase boundary, represented in Figs. 16a and b.

Viewed along the $[10\bar{1}]_{cal}$ zone (Fig. 9b) the structure consists of $AuTe_2$ and $AgTe_2$ columns forming again a square grid. The image consists of bright dots the configuration of which, in size as well as in orientation, corresponds with that of the columns in the model (Fig. 17b). It is quite clear that the brightness of the rows of dots is modulated with a period which in the commensurate structure (see Fig. 1) is equal to four times the distance between horizontal rows, i.e., $4d_{202}$, whereas in the incommensurate one it is more like four and a half times the same distance. Also in the incommensurate phase the lines of bright dots are not exactly parallel with the [010] direction which is consistent with the orientation anomaly in the diffraction pattern (Fig. 4d). The antiphase boundaries are not clearly revealed in this section presumably because there is no visible displacement of dot rows on either side of the interface. However, on close examination of the dot intensities it turns out that the brightest dots provide direct evidence for a displacement vector of the type $1/4\,[021]_{sylv} = 1/2\,[110]_{cal}$. A model for the antiphase boundary, as viewed along this direction, is shown in Fig. 17; it can be compared with the pattern of unit cells marked on the photograph of Fig. 9b. Regular ledging of the APB's may cause an orientation anomaly which is coupled to the orientation anomaly in the [202] sequences of satellites. Also the distance between

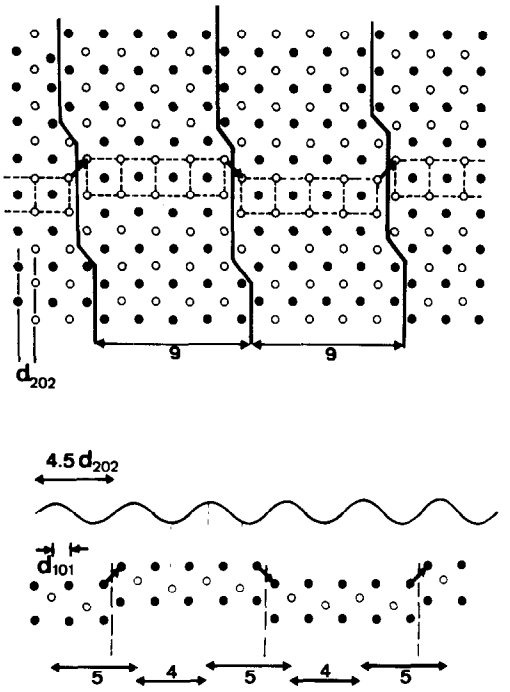

FIG. 17. (a) The coupling between a displacement wave with period 4.5 d_{202} in the superstructure and the periodic antiphase boundary arrangement. The displacements of the silver containing columns (open circles) are exaggerated. The average period of the deformation wave is 4.5 whereas the distance between APB's is twice as large in this case. (b) View of the periodic antiphase boundary structure as viewed along the $[10\bar{1}]_{cal}$ direction. The full dots represent $AuTe_2$ columns, whereas the open circles represent $AgTe_2$ columns. The vector is $1/2[110]_{cal}$. Systematic ledging of the antiphase boundaries causes an orientation anomaly.

APB's is somewhat variable: it is either eight or nine d_{202} layers (Figs. 16a, 17a). The incommensurability of the deformation modulation is due to a mixture of spacings 5 and 4 (Fig. 17a); note that the average period (~4.5) is related to that of the deformation modulation in calaverite.

The diffraction pattern along the $[\bar{1}3\bar{2}]$ zone (Fig. 7a) presents satellites alone the $[20\bar{1}]$ direction. This sequence of satellites is consistent with the (010) reciprocal lattice plane represented in Fig. 3 (line a). The sequence along $[20\bar{1}]$ is formed by two third order satellites and their second order satellites possibly produced by double diffraction. The corresponding image (Fig. 18) reveals a square array of bright dots. Somewhat brighter lines give the image a modulated aspect; their period is a mixture of two and three times the spacing between rows of dots. The largest part of the sequence can be represented by the succession of number 3 3 3 2 3 3 3 2 ... regularly intermixed with 3 3 2. The same type of sequence is found in other sections containing the $[20\bar{1}]$ sequences of satellites. This corresponds with the fact that the distance from the $[20\bar{1}]$ spot to the origin is divided in 2.75 parts by the satellites; 2.75 is clearly the average of 3, 3, 3, and 2.

The structural significance of this modulation is not immediately obvious. It should be noted that this modulation is not observed in the [010] section; there is evidence neither in the image nor in the diffraction pattern along this zone. This is due to the fact that the modulation is produced by third order satellites which are absent in the [010] zone.

Third order satellites of the [202] sequences are moreover weak in other sections. A very well-defined modulation due to the $[20\bar{1}]$ sequence of satellites is represented in Fig. 19, the 3 3 3 2 sequence of atom layers is clearly visible.

In the [102] zone image the structure is viewed along a direction which is almost exactly perpendicular to the planes of equal phase of the [202] modulation. The pattern consists of a square array of dots. Rather ill-defined bright lines cause a grouping of the rows of dots in sets of three or two. The observed subperiod in Fig. 18 corresponds with the succession of $(10\bar{2})$ atom planes each containing the three types of atoms (Fig. 1). These planes are indicated schematically in Fig. 23 by short segments. From the drawing it is clear that the period of the modulated structure in this direction,

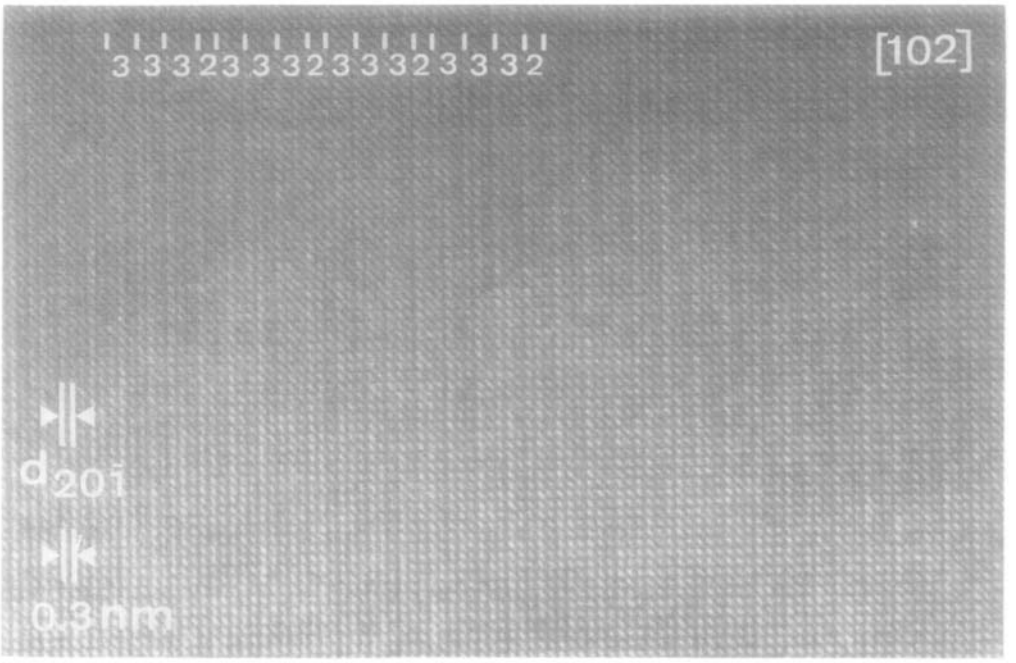

FIG. 18. View along the $[\bar{1}3\bar{2}]$ zone of the modulated sylvanite structure.

which is parallel with the a_{sylv} direction, contains 10 to 11 atom planes. This is consistent with the observed modulation period of 3 + 3 + 3 + 2 = 11 atom planes. This period is not strictly constant, however; a sequence of 3 3 2 is periodically intermixed (Fig. 18). The grouping in three, sometimes two, rows of atom columns, separated by a brighter line (Fig. 18) is most probably related to the fact that the period of the pattern of the tellurium displacements in the a_{sylv} direction contains three atomic planes (Fig. 1). In other zones, containing the $[20\bar{1}]$ satellite sequences, the same period and the same grouping occurs, although the viewing directions are different, of course.

It may be concluded that the observed superperiod in images along these zones reflects the superperiod caused by the antiphase boundaries.

6. Image Simulations

We have produced computer generated images for a number of zones of the ideal sylvanite structure, using a method developed by D. Van Dijck (*4*). The method takes into account dynamical diffraction effects and corrects for the instrumental factors. The final computed image is displayed on a cathode ray screen and photographed. Computed and observed images thus have similar aspects because they are of the same nature. The C_s value of the electron microscope used was C_s = 1.2 nm.

The effect of the presence of antiphase boundaries along the viewing direction on the contrast of the image has been shown to be limited to the first rows of atom columns adjacent to the interface, in sufficiently thin crystals. The images within the domains are thus the same as those of the unperturbed

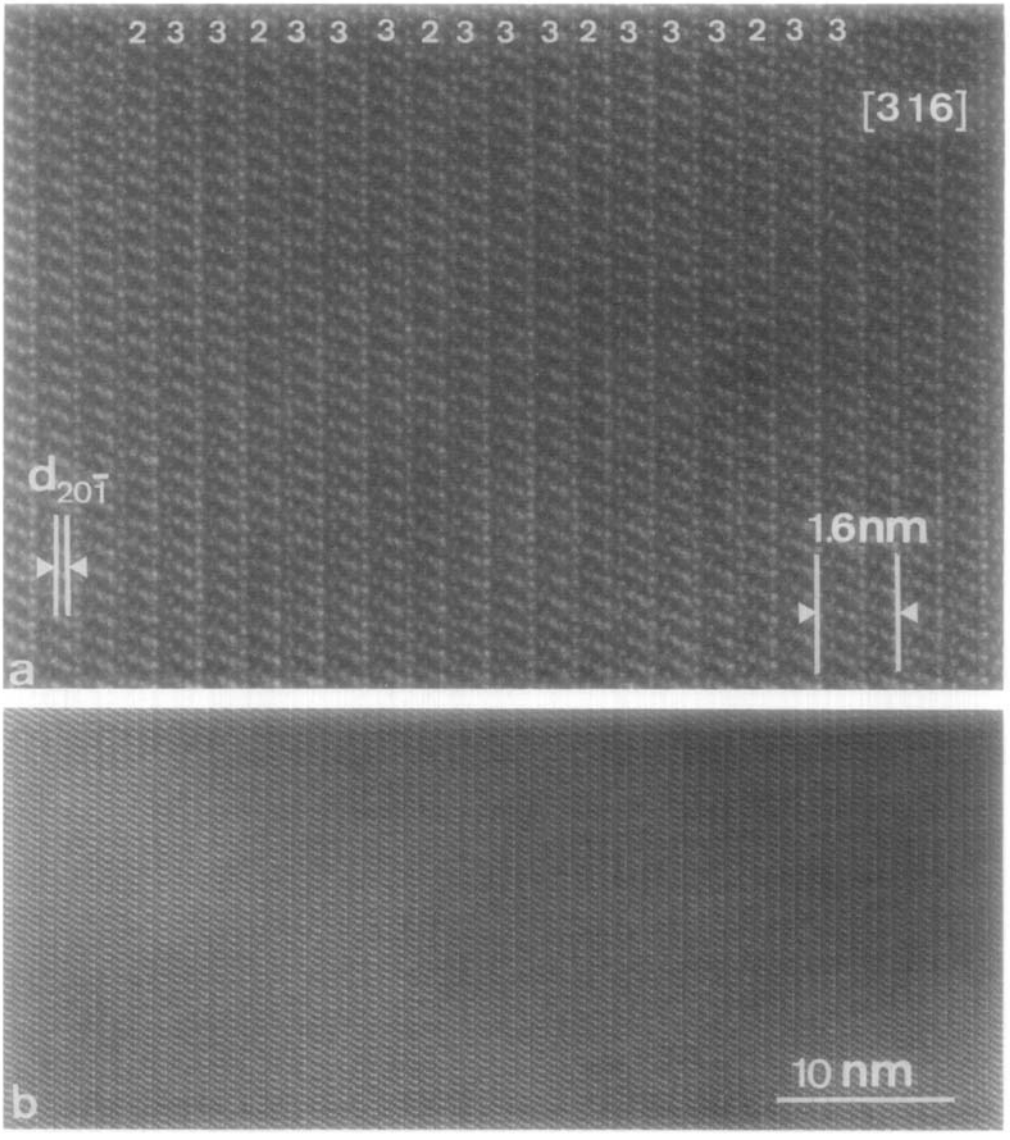

FIG. 19. View along the [316] zone of the modulated sylvanite structure. Interfaces are revealed by brighter lines; the spacing is regularly mixed according to the sequence 3 3 3 2. Systematic ledging causes an orientation anomaly.

structure (*5*). It is therefore sufficient to compute images of the ideal structure; one can extrapolate the results with confidence to interface fragmented long period structures. For each zone we calculated a matrix of images corresponding with different thicknesses and defocus values.

The computer generated images for the [010] zone are reproduced in Fig. 20 for three thicknesses: 5, 10, and 20 nm, and four defocus values: −80, −90, −100, and −110 nm. For all images the lower left corner is occupied by a gold column. In most images gold and silver columns are re-

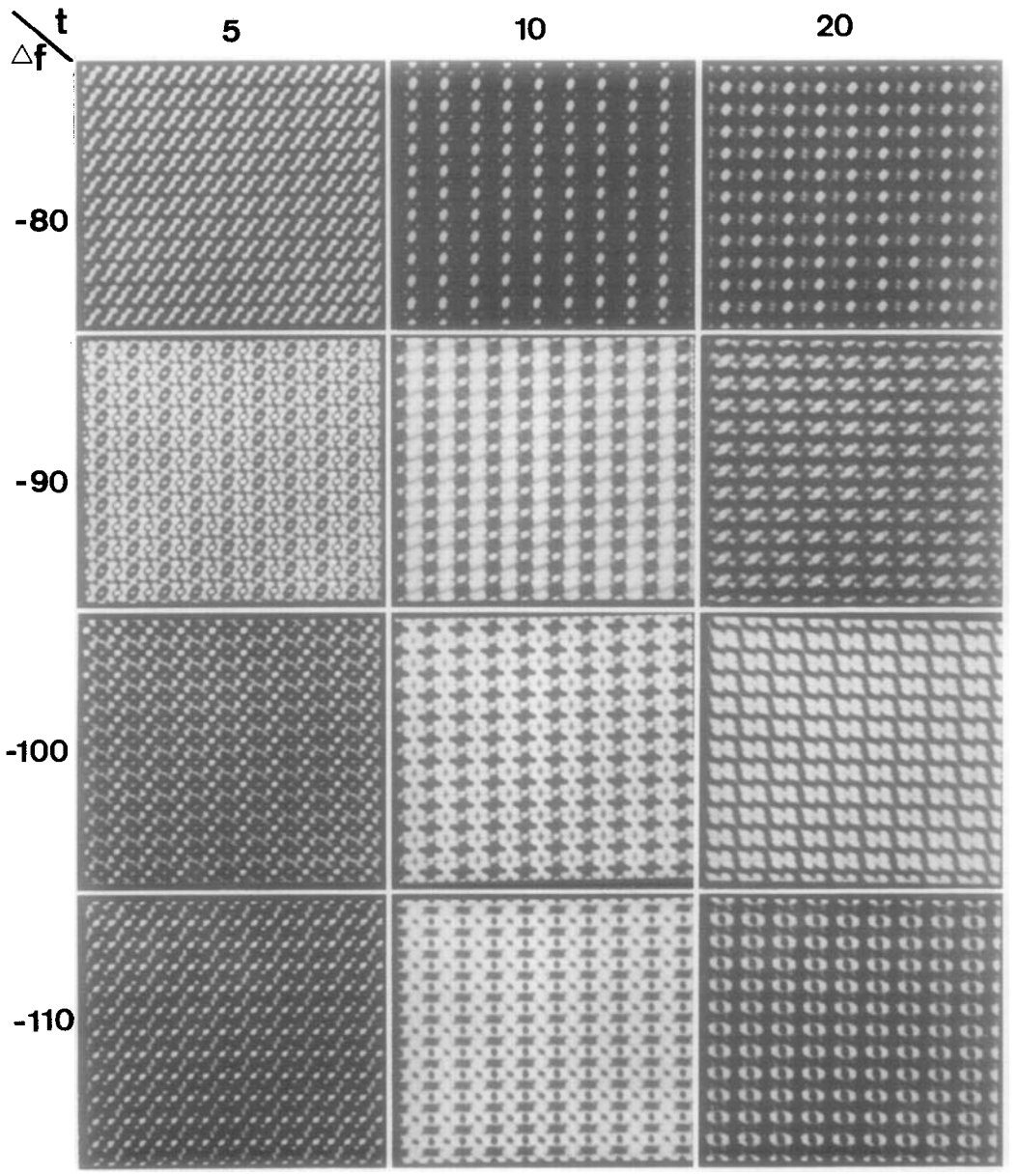

FIG. 20. Matrix of simulated images along the [010] zone for different thicknesses and defocus values (C_s = 1.2 nm). These images can be compared with the observed images of Fig. 8. In all the images a gold column was put in the lower left corner.

vealed as the brightest dots, whereas the tellurium columns are marked by weaker dots. In some of the images, e.g., t = 10 nm and f = −80 nm the gold atom columns only are revealed as the brightest dots.

The calculated images can be compared with the experimental ones reproduced as Fig. 8. Figures 8a and b, which are from the same area, imaged with a different focus but with a thickness of 5 nm and defocus

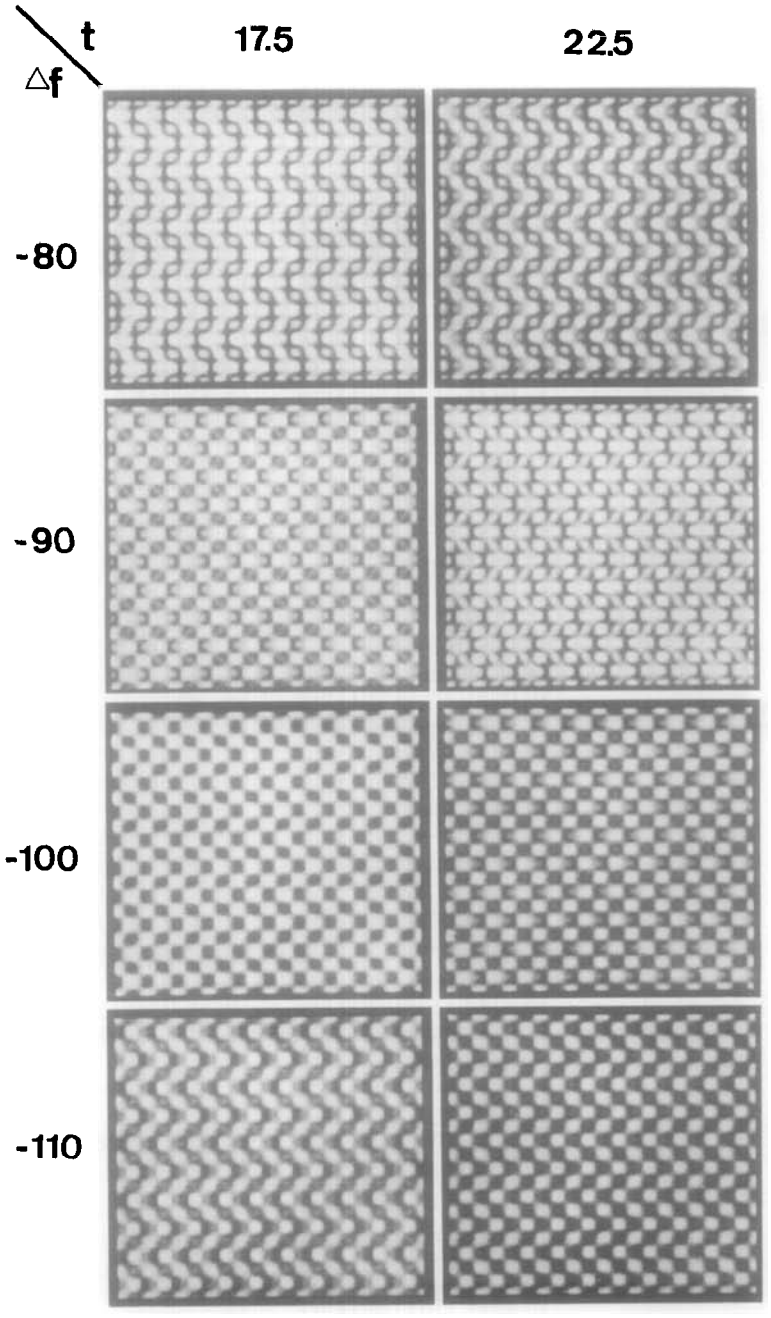

FIG. 21. Matrix of simulated images along the [10$\bar{1}$] zone for different thicknesses and defocus values in nanometers (C_s = 1.2 nm). The image can be compared with the observed images of Fig. 9a. A gold column was put in the lower left column.

values of −80 and −110 nm, respectively.

Figure 8c is from a thicker area and compares well with the calculated image at a thickness of 20 nm and −80-nm defocus value.

In Fig. 21 we have reproduced a matrix

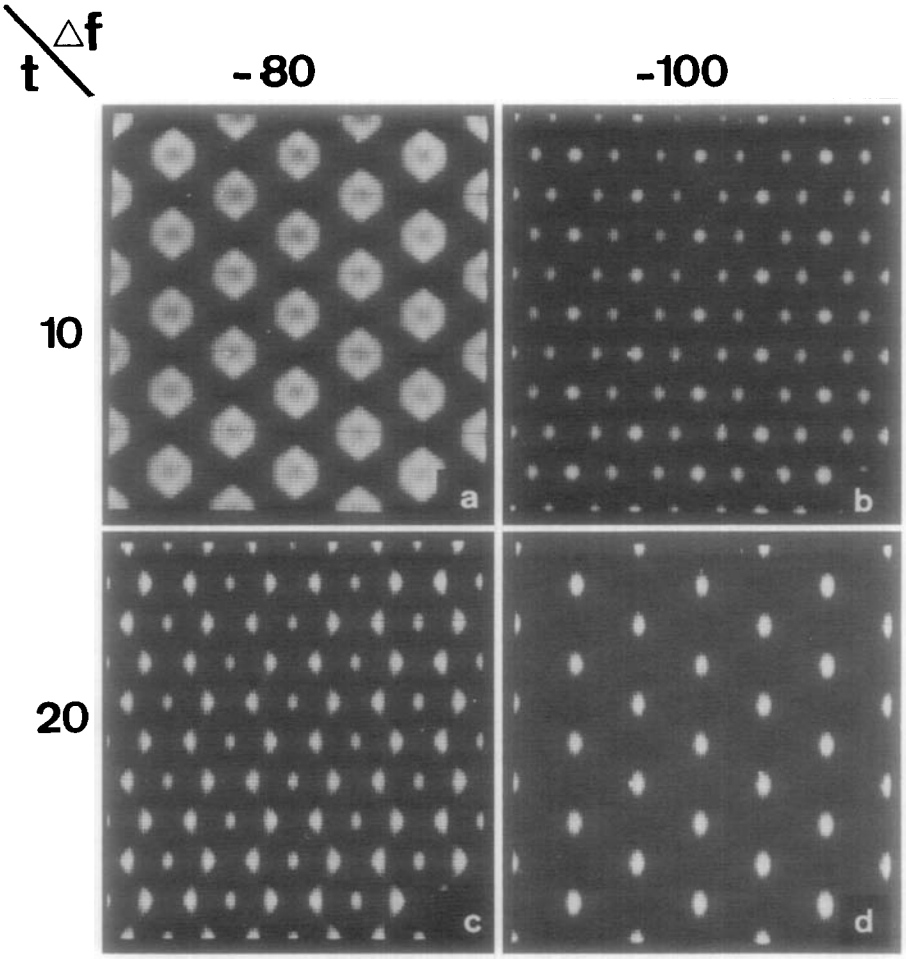

FIG. 22. Matrix of simulated images along the $[001]_{cal}$ zone for different thicknesses and defocus values (expressed in nm). For $t = 10$ nm and $\Delta f = -100$ nm, the difference between heavy metal and tellurium columns is quite evident. Compare with Fig. 10.

of images of the structure as viewed along the [101] zone. There is only a small difference in contrast between $AuTe_2$ and $AgTe_2$ columns. The true period of the projected structure can best be observed for $t = 17.5$ nm and $f = -110$ nm and for $t = 22.5$ nm and $f = -80$ nm. In the latter image the alternating levels of the silver atoms are clearly visible. These computer generated images can be compared with the actually observed image of Fig. 9a.

Figure 22 shows computer simulated images along the $[001]_{cal}$ zone. The difference between heavy metal and tellurium columns can clearly be seen in Fig. 22 for $t = 10$ nm and $f = -100$ nm. This computed image can be compared with the observed image of Fig. 10. At other defocus values only the heavy metal configuration is imaged.

7. Discussion

It is surprising to find that the substitution of gold by silver in $AuTe_2$ in a rather

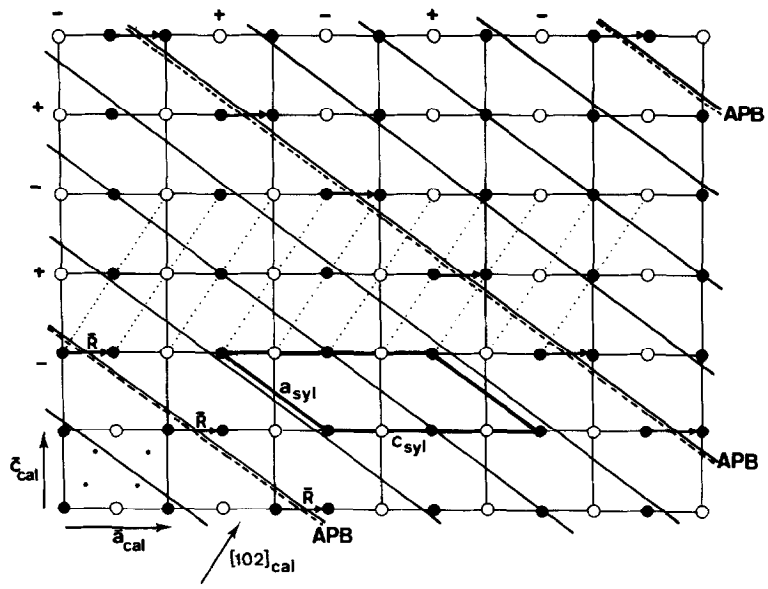

FIG. 23. Model for the incommensurate sylvanite structure as viewed along the [010] zone. Zeros of the modulation wave are marked by full lines. The APB's are marked by dashed lines. Along the APB's vertical rows of silver columns (open circles) interchange with rows of gold columns (full circles); tellurium columns are not shown.

broad composition range around the ratio 1 : 1 changes neither the period of the modulation, nor its direction to a large extent, except when the composition comes very close to $AuAgTe_4$. In the latter case the commensurate sylvanite structure results.

This behavior is presumably due to the fact that this substitution does not affect the electron/atom ratio and, moreover, the fact that the atomic radii of silver and gold are very closely equal (0.144 nm). Since in commensurate sylvanite with composition $AuAgTe_2$ silver and gold are ordered in such a way that silver atoms occupy the extrema of the modulation wave (i.e., the crests and the throughs) whereas the gold atoms occupy the zeros, it is reasonable to assume that also in the incommensurate phase the silver atoms will tend to occupy the extrema of the modulation wave. However, since the wavelength of the modulation wave is now incommensurate with the distance between gold and silver atoms this simple rule cannot be exactly satisfied, except in a limited number of lattice sites.

It is thus reasonable to assume that the ordering in nonstoichiometric incommensurate sylvanite occurs according to the following principle: An atomic position which comes closer to a zero than to an extremum of the displacement wave will be occupied preferentially by a gold atom, whereas an atomic position which comes closer to an extremum than to a zero will be occupied preferentially by a silver atom. Applying this simple rule to a displacement wave with wavelength 4.5 d_{101} leads to a structure in which the gold and silver atoms occupy the positions as represented in a view along the $[10\bar{1}]$ sylvanite direction (Fig. 17b) and along [010] in Fig. 23. It is clear that the structure now contains some interfaces which can to a good approximation be considered as antiphase boundaries with a displacement vector $1/2\ [110]_{cal} \equiv 1/4\ [021]_{sylv}$. The high resolution images (Fig. 9b) pro-

vide in fact direct evidence for the occurrence of interfaces with this displacement vector. This periodic antiphase boundary structure conserves the same average period of 4.5 d_{101} of the modulation wave (Fig. 17b) and it therefore only affects the intensities of the satellites but does not affect their positions. This explains why the satellite sequences appear enhanced in incommensurate sylvanite; apart from the modulation due to displacements there is also structure factor modulation now.

One may wonder how this periodic antiphase boundary structure is revealed in the [010] zone diffraction pattern. Although the [010] zone diffraction patterns of calaverite and of incommensurate sylvanite have the same geometry, their interpretation is different. In the case of calaverite the pairs of weak spots around the positions of absent spots of the type $h0l$ (with h = odd) have been attributed to the second order spots caused by the modulation wave. In the case of sylvanite the same spots can moreover be interpreted as being due to the splitting of the $h0l$ (h = odd) basic spots of sylvanite (in calaverite indices) as a result of the introduction of periodic antiphase boundaries (Fig. 3). The fractional displacement is 1/2 for such spots (h = odd) and it is 0, for the other basic spots. This is consistent with the displacement vector of the type $R = \frac{1}{2}[110]_{cal} \equiv \frac{1}{4}[021]_{sylv}$ postulated for these antiphase boundaries, since the fractional shift is given by $\bar{g} \cdot \bar{R}$ (*6*). Also the separation of these pairs of spots as well as the direction of their connecting line is consistent with the direction and spacing of the periodic APB structure.

The high resolution images (Fig. 9b) show that the spacing of the APB structure is not strictly constant but somewhat variable. The spacing observed in the diffraction pattern is thus an average: this is presumably also the reason why usually only two satellites are observed in the section producing the APB images. Although in sylvanite one observes sometimes sequences of up to eight equidistant satellites in the $20\bar{2}$ sequences; in calaverite this has never been found to be the case as yet.

The presence of the second order satellite in the [010] zone is the consequence of the fact that the tellurium positions are modulated according to a pattern of which the unit mesh in the (010) plane has only half the surface area of that of the modulation pattern of the silver positions. Whereas the displacements of the silver atoms are all in the [010] direction, the displacements of the Te atoms have also a component parallel to the (010) plane. The satellites in the [010] section therefore only result from the tellurium contribution; the silver atom displacements do not at all cause satellites in this section.

All diffraction patterns of the incommensurate phase can thus be explained in a consistent manner on the basis of the reciprocal lattice of which the (010) plane is represented in Fig. 3 and which is quite similar to the corresponding reciprocal lattice of calaverite. This means that the modulated structure of sylvanite must be very closely related to that of calaverite. In postulating a model for the incommensurate modulated structure of sylvanite we can find an indication in the commensurate structure derived by Tunell and Pauling (*2*). In the latter model the modulation period contains four $(101)_{cal}$ layers, whereas in the incommensurate structure it should be equal to ~4.5 times the distance between (101) layers; the orientation of the planes of equal phase should be slightly different from (101). The levels of the gold and silver atoms could thus be represented as in Fig. 17, in a view along the $[10\bar{1}]_{cal}$ zone and in projection on the (010) plane in Fig. 23. Note that this model is consistent with the high resolution image of Fig. 13; along the APB's rows of silver columns interchange with rows of gold columns parallel with c_{cal}.

Conclusion

Sylvanite ($Au_{1+x}Ag_{1-x}Te_4$) may occur both as a commensurate and as an incommensurate structure. It is suggested that the commensurate form has the ideal composition $AuAgTe_4$ and adopts the structure determined by Tunell and Pauling (*2*), which can be considered as a commensurate deformation modulated derivative of a cubic structure. The incommensurate deformation modulated structure is closely related to that of calaverite $AuTe_2$, discussed in Part I. The substitution of gold by silver in the vicinity of the 1 : 1 ratio does not affect the period of the deformation modulated structure to any great extent, but introduces simultaneously a long period antiphase boundary modulated structure, of which the period is closely coupled with that of the deformation modulated structure. Along the antiphase boundaries excess gold can be incorporated in sylvanite without changing the period by the formation of thin layers of calaverite-like structure.

The modulation in nonstoichiometric sylvanite turns out to be a remarkable combination of a displacement wave coupled with interface modulation by means of a long period antiphase boundary arrangement. High resolution electron microscopy combined with electron diffraction has proved to be an essential tool in elucidating this complicated coupling of two modulation modes.

References

1. G. Van Tendeloo, P. Gregoriades, and S. Amelinckx, *J. Solid State Chem.* **50,** XXX (1983).
2. G. Tunell and L. Pauling, *Acta Crystallogr.* **5,** 375 (1952).
3. J. Van Landuyt, G. Van Tendeloo, and S. Amelinckx, *Phys. Status Solidi* A, **26,** K9 (1974).
4. D. Van Dyck, *J. Microsc.* **119,** 141 (1980).
5. H. Matsuhata *et al.,* to be published.
6. J. Van Landuyt, R. De Ridder, R. Gevers, and S. Amelinckx, *Mater. Res. Bull.* **5,** 353 (1970).